

Article

Optimal Siting and Sizing of Hydrogen Production Modules in Distribution Networks with Photovoltaic Uncertainties

Zhiyong Li ¹, Wenbin Wu ^{2,*}, Yang Si ²  and Xiaotao Chen ²

¹ Department of Computer Technology and Application, Qinghai University, Xining 810016, China; lizy@qhu.edu.cn

² Qinghai Key Lab of Efficient Utilization of Clean Energy, School of Energy and Electrical Engineering, University of Qinghai, Xining 810016, China; siyang@qhu.edu.cn (Y.S.); chenxiaotao@qhu.edu.cn (X.C.)

* Correspondence: wuwenbin1123@qhu.edu.cn; Tel.: +86-13709750818

Abstract: Hydrogen production modules (HPMs) play a crucial role in harnessing abundant photovoltaic power by producing and supplying hydrogen to factories, resulting in significant operational cost reductions and efficient utilization of the photovoltaic panel output. However, the output of photovoltaic power is stochastic, which will affect the revenue of investing in an HPM. This paper presents a comprehensive analysis of HPMs, starting with the modeling of their operational process and investigating their influence on distribution system operations. Building upon these discussions, a deterministic optimization model is established to address the corresponding challenges. Furthermore, a two-stage stochastic planning model is proposed to determine optimal locations and sizes of HPMs in distribution systems, accounting for uncertainties. The objective of the two-stage stochastic planning model is to minimize the distribution system's operational costs plus the investment costs of the HPM subject to power flow constraints. To tackle the stochastic nature of photovoltaic power, a data-driven algorithm is introduced to cluster historical data into representative scenarios, effectively reducing the planning model's scale. To ensure an efficient solution, a Benders' decomposition-based algorithm is proposed, which is an iterative method with a fast convergence speed. The proposed model and algorithms are validated using a widely utilized IEEE 33-bus system through numerical experiments, demonstrating the optimality of the HPM plan generated by the algorithm. The proposed model and algorithms offer an effective approach for decision-makers in managing uncertainties and optimizing HPM deployment, paving the way for sustainable and efficient energy solutions in distribution systems. Sensitivity analysis verifies the optimality of the HPM's siting and sizing obtained by the proposed algorithm, which also reveals immense economic and environmental benefits.

Keywords: hydrogen production; two-stage stochastic programming; optimal planning; data-driven algorithm; Benders' decomposition



Citation: Li, Z.; Wu, W.; Si, Y.; Chen, X. Optimal Siting and Sizing of Hydrogen Production Modules in Distribution Networks with Photovoltaic Uncertainties. *Energies* **2023**, *16*, 7636. <https://doi.org/10.3390/en16227636>

Academic Editor: Angela Russo

Received: 17 October 2023

Revised: 12 November 2023

Accepted: 14 November 2023

Published: 17 November 2023



Copyright: © 2023 by the authors. Licensee MDPI, Basel, Switzerland. This article is an open access article distributed under the terms and conditions of the Creative Commons Attribution (CC BY) license (<https://creativecommons.org/licenses/by/4.0/>).

1. Introduction

Power-to-hydrogen (P2H) is increasingly recognized as an effective solution to address the challenges of renewable energy consumption in both theoretical research and engineering demonstrations [1,2]. By converting electrical energy into chemical energy stored in hydrogen through hydrogen production modules (HPMs), P2H enables a significant increase in the utilization rate of renewable energy in power systems. Moreover, the produced hydrogen finds diverse applications in transportation [3,4], heating [5], chemical industry [6], and other fields. However, the impact of HPMs on distribution systems containing a high proportion of renewables, especially their impacts on sizing and siting problems, is still limited.

The integration of HPMs into power systems offers notable advantages in two key aspects. Firstly, HPMs present distinct application benefits compared to energy-based storage technologies like battery energy storage. Functioning as power-oriented components

capable of accommodating ultra-large capacities [7–9], HPMs enhance the operational efficiency of distribution systems. Furthermore, the versatile usability of the produced hydrogen across various industries expands its potential applications [6,10]. Secondly, HPMs can serve as controllable loads within the power grid, capitalizing on their energy conversion volume and rapid response capabilities [11,12]. Active participation of HPMs in peak regulation [13] and frequency regulation [14,15] services contributes to the improved flexibility of power system operations. In summary, HPMs play a crucial role in power systems, enhancing operational efficiency, enabling diverse industrial applications for hydrogen, and serving as controllable loads that enhance the grid's flexibility.

The optimization of site selection and capacity determination for HPM modules has gained our attention, considering the substantial benefits of their integration into power distribution systems. The siting and sizing of HPMs pose significant challenges within power distribution systems. The siting problem necessitates comprehensive consideration of multiple factors, including power network topology, transmission line capacities, and land constraints [16–18]. Likewise, sizing HPMs requires accurate estimation of future demands, considering factors such as load variations, renewable energy integration [19–21], and the increasing trend of hydrogen demands. Additionally, uncertainties, such as the volatility of renewable energy and market demand, further complicate sizing decisions [22,23].

Although numerous studies have been conducted on the integration and operation of HPMs in power distribution systems, limited attention has been given to the site selection and capacity determination of HPMs. Some studies have explored the cooperation between renewables and HPMs [24–26], while others have proposed optimal energy management strategies, utilizing HPMs to support renewable energy consumption [27,28]. Some studies also considered the integration of electrolyzers and fuel cells and introduced them into the system operations [29–32].

When dealing with the uncertainty, there are mainly three methodologies, stochastic optimization [33–35], robust optimization [36–38], and distributionally robust optimization [39–41]. Robust optimization methods build uncertainty sets to guarantee the feasibility of the worst-case scenario, whose solution is regarded as too conservative. Distributionally robust optimization methods develop ambiguity sets to make sure that the scenario with the worst-case distribution can be maintained. Both types of methods are too conservative and may lose much information from historical data when formulating uncertainty or ambiguity sets. Meanwhile, both of them may face the curse of dimensionality since auxiliary binary variables are commonly introduced into the mathematical model. On the contrary, stochastic models can directly utilize historical data, and their mathematical structures are quite simplified. Therefore, in this paper, a stochastic optimization model is selected.

Another problem is how to effectively solve the stochastic siting and sizing problem of HPM. There will be large-scale historical data, which extremely increases the scale of the optimization problem. Bender's decomposition has been widely applied in the existing literature [42–44]. It can decompose the optimization problem into subproblems, which have much smaller scales and can be solved in parallel. Compared to robust-based methods [36–41], Bender's decomposition can achieve faster computation speed. In this paper, a data-driven K-means algorithm is utilized to reduce the scale of scenarios, which further accelerates the solving speed.

Recognizing the research gap regarding site selection and capacity determination, our study aims to address these issues. The contributions of our research are twofold:

- An optimal location and capacity model for hydrogen production modules (HPMs) is formulated using a two-stage stochastic programming approach. The model explicitly considers uncertainties related to renewable energy availability and load fluctuations, while also incorporating operation and investment costs during the planning phase.
- To efficiently solve the siting and sizing problem, a Bender's decomposition-based algorithm is devised. Additionally, a data-driven stochastic programming scene reduction method is developed to address the challenge of low efficiency associated with the presence of integer variables in the two-stage stochastic programming problem.

These proposed methods enhance the effectiveness and computational efficiency of the optimization process.

In the following, Section 2 establishes a detailed two-stage stochastic planning model for the hydrogen production module in distribution systems with large-scale renewable power. Section 3 proposes an algorithm based on the Benders' decomposition to solve the proposed two-stage stochastic planning model, while Section 4 proposes a data-driven clustering method to generate typical scenarios from massive historical data. Section 5 discusses the numerical experiments. Section 6 concludes the work.

2. Sizing and Siting of Hydrogen Production Modules

In this paper, we assume that there is one HPM to be invested in. We will decide the capacity and the location of the HPM to minimize the operational cost of the distribution system plus the investment cost of the HPM. In this section, we develop the two-stage stochastic planning optimization model of the HPM. In stage 1, we decide the capacity and the location of the HPM. In stage 2, after the HPM has been built, the daily operations of the distribution system are simulated at a set of typical scenarios. The objective is to choose the optimal capacity and location of the HPM to minimize the sum of the investment cost of the HPM and the operational cost of the distribution system. The two-stage stochastic planning problem of the HPM will be formulated in this section, while the generation of typical scenarios will be developed in the next section.

Denote by $\mathcal{S} = \{1, 2, \dots, S\}$, the set of typical scenarios, indexed by s . Each scenario s differs from the maximal power profile of photovoltaic (PV) panels and the load profile. Denote by $\mathcal{T} = \{1, 2, \dots, T\}$, the set of time intervals in a day, indexed by t . In the targeted distribution system, there are $1 + N$ buses indexed by $\mathcal{N} = \{0, 1, 2, \dots, N\}$. Let $\mathcal{E} \subseteq \mathcal{N} \times \mathcal{N}$ denote the set of distribution lines.

2.1. Hydrogen Production Module Model

The long time-scale investment in the HPM simultaneously considers its capacity and location. The capacity of HPM means its rated power \bar{P}^{HPM} . The operational constraints of the HPM include the power limitation

$$\eta^{\min} \bar{P}^{HPM} \leq P_{s,t}^{HPM} \leq \bar{P}^{HPM}, \quad s \in \mathcal{S}, t \in \mathcal{T} \quad (1)$$

and the ramping limitation

$$-\eta^{\text{ramp}} \bar{P}^{HPM} \leq P_{s,t}^{HPM} - P_{s,t-1}^{HPM} \leq \eta^{\text{ramp}} \bar{P}^{HPM}, \quad s \in \mathcal{S}, t = 2, 3, \dots, T \quad (2)$$

where $P_{s,t}^{HPM}$ is the power consumption of the HPM in scenario s at time interval t , $\eta^{\min} \bar{P}^{HPM}$ is the minimal power consumption of the HPM, and $\eta^{\text{ramp}} \bar{P}^{HPM}$ is the maximal ramping power.

It is revealed that the rated power \bar{P}^{HPM} determines the flexibility of HPM. The annual investment cost of HPM discounted each year is given by

$$C^{INV} = \eta^{ADF} \pi_{HPM} \bar{P}^{HPM}. \quad (3)$$

where π^{HPM} is the unit investment price of the HPM, and η^{ADF} is the annuity depreciation factor defined as

$$\eta^{ADF} = \frac{\eta^{DR} (1 + \eta^{DR})^{Y^{EP}}}{(1 + \eta^{DR})^{Y^{EP}} - 1} \quad (4)$$

In (4), the factor η^{DR} is the discount rate and Y^{EP} is the expected life span of HPM in years.

The location of the HPM in the distribution system is another significant decision. Use the binary variable u_i to describe the siting process

$$P_{i,s,t}^{HPM} = u_i P_{s,t}^{HPM}, i \in \mathcal{N}, s \in \mathcal{S}, t \in \mathcal{T} \quad (5)$$

where u_i is a binary variable and $P_{i,s,t}^{HPM}$ is an auxiliary variable. The binary variable $u_i = 1$ if the HPM is sited at bus i , and $u_i = 0$ if not. Since there is only one HPM, the binary variable u_i should be restricted to

$$\sum_{i \in \mathcal{N}} u_i = 1, \quad (6)$$

$$u_i \in \{0, 1\}, i \in \mathcal{N} \quad (7)$$

Note that the constraint (5) is intractable since there is a bilinear term $u_i P_{s,t}^{HPM}$. By the big-M method, the constraint can be replaced with

$$i \in \mathcal{N}, s \in \mathcal{S}, t \in \mathcal{T} : \quad (8a)$$

$$-Mu_i \leq P_{i,s,t}^{HPM} \leq Mu_i$$

$$M(u_i - 1) \leq P_{i,s,t}^{HPM} - P_{s,t}^{HPM} \leq M(1 - u_i) \quad (8b)$$

where $M > 0$ is a sufficiently large constant.

When the HPM is equipped, it can produce hydrogen using electricity. The hydrogen production rate is given by

$$n_{s,t} = \eta^{HPR} P_{s,t}^{HPM} \quad (9)$$

where η^{HPR} is the hydrogen production rate by unit power. The produced hydrogen can be sold to chemical plants. The revenue for each typical scenario s is defined as

$$R_s^{HT} = \pi^{HTP} \sum_{t \in \mathcal{T}} n_{s,t} \quad (10)$$

where π^{HTP} is the hydrogen trading price.

2.2. Distributed Generator Model

There are two types of distributed generator modules integrated into the distribution system: fuel generator and PV panel. In this work, we take the PV as an example to describe the uncertainties induced by renewables. Of course, our model is scalable and can also be applied to other renewable energy sources.

Fuel generators are fully controllable. The set of buses with a fuel generator is denoted by $\mathcal{G} \subseteq \mathcal{N}$. For the fuel generator at bus $i \in \mathcal{G}$, its operational constraints include the minimal/maximal generation output limitation

$$\underline{P}_i^G \leq P_{i,s,t}^G \leq \bar{P}_i^G, i \in \mathcal{G}, s \in \mathcal{S}, t \in \mathcal{T} \quad (11)$$

and the ramping limitation

$$-R_i^G \leq P_{i,s,t}^G - P_{i,s,t-1}^G \leq R_i^G, i \in \mathcal{G}, s \in \mathcal{S}, t = 2, 3, \dots, T \quad (12)$$

where $P_{i,s,t}^G$ is the power output of the fuel generator at bus i in scenario s at time interval t , \underline{P}_i^G and \bar{P}_i^G are the minimal and maximal power output of the fuel generator at bus i , and R_i^G is the maximal ramping power of the fuel generator at bus i .

The generation cost of a fuel generator is a quadratic function as

$$C_{i,s}^G = \sum_{t \in \mathcal{T}} a_i (P_{i,s,t}^G)^2 + b_i P_{i,s,t}^G + c_i, \quad i \in \mathcal{G}, s \in \mathcal{S} \quad (13)$$

where $a_i > 0$, b_i , and c_i are constant.

PV panels can only be cut down from their maximal power output. The set of buses with a PV panel is denoted by $\mathcal{V} \subseteq \mathcal{N}$. In scenario s , the maximal power output of the PV panel $i \in \mathcal{V}$ at time interval t is $\bar{P}_{i,s,t}^{PV}$. The operational constraint of the PV panels is

$$0 \leq P_{i,s,t}^{PV} \leq \bar{P}_{i,s,t}^{PV}, \quad i \in \mathcal{V}, s \in \mathcal{S}, t \in \mathcal{T} \quad (14)$$

where $P_{i,s,t}^{PV}$ is the real power output of the PV panel at bus i in scenario s at time interval t .

The cost of a PV panel is the penalty for the curtailment of PV power

$$C_{i,s}^{PV} = d_i (\bar{P}_{i,s,t}^{PV} - P_{i,s,t}^{PV}), \quad i \in \mathcal{V}, s \in \mathcal{S} \quad (15)$$

where d_i is a positive constant.

2.3. Power Flow Model

From [45], the distribution flow (DistFlow) model is given for each line $(i, j) \in \mathcal{E}$, $s \in \mathcal{S}$, $t \in \mathcal{T}$ as

$$P_{ij,s,t} = P_{j,s,t}^D - P_{j,s,t} + r_{ij} I_{ij,t} + \sum_{(j,k) \in \mathcal{E}} P_{jk,s,t} \quad (16a)$$

$$Q_{ij,s,t} = Q_{j,s,t}^D + x_{ij} I_{ij,t} + \sum_{(j,k) \in \mathcal{E}} Q_{jk,s,t} \quad (16b)$$

$$U_{i,s,t} - U_{j,s,t} = 2(r_{ij} P_{ij,s,t} + x_{ij} Q_{ij,s,t}) - (r_{ij}^2 + x_{ij}^2) I_{ij,t} \quad (16c)$$

$$I_{ij,s,t} U_{i,s,t} = P_{ij,s,t}^2 + Q_{ij,s,t}^2 \quad (16d)$$

where $P_{ij,s,t}$, $Q_{ij,s,t}$, and $I_{ij,t}$ are the active power, the reactive power, and the squared magnitude of the current from bus i to bus j in scenario s at time interval t ; r_{ij} and x_{ij} are the resistance and reactance of distribution line (i, j) ; $P_{j,s,t}^D$, $Q_{j,s,t}^D$, $P_{j,s,t}$, and $U_{j,s,t}$ are the uncontrollable active load, the uncontrollable reactive load, the controllable active power injected, and the squared magnitude of the voltage at bus j in scenario s at time interval t .

Note that the constraint (16d) is non-convex. By [46], the net loss is much smaller than the line power and, hence, can be ignored. This simplification derives the linear distribution flow (LinDistFlow) model

$$P_{ij,s,t} = P_{j,s,t}^D - P_{j,s,t} + \sum_{(j,k) \in \mathcal{E}} P_{jk,s,t} \quad (17a)$$

$$Q_{ij,s,t} = Q_{j,s,t}^D + \sum_{(j,k) \in \mathcal{E}} Q_{jk,s,t} \quad (17b)$$

$$U_{i,s,t} - U_{j,s,t} = 2r_{ij} P_{ij,s,t} + 2x_{ij} Q_{ij,s,t} \quad (17c)$$

In the LinDistFlow model (17), the controllable active power injected $P_{j,s,t}$ is defined for each bus $j \in \mathcal{N}$ as

$$P_{j,s,t} = \mathbf{1}_{(j \in \mathcal{G})} P_{j,s,t}^G + \mathbf{1}_{(j \in \mathcal{V})} P_{j,s,t}^{PV} - P_{i,s,t}^{HPM} \quad (18)$$

where $\mathbf{1}_{(\cdot)}$ is the indicator function. $\mathbf{1}_{(j \in \mathcal{G})}$ is one if $j \in \mathcal{G}$ and zero if $j \notin \mathcal{G}$. The definition of $\mathbf{1}_{(j \in \mathcal{V})}$ is similar.

Bus 0 is connected to the transmission system, whose voltage is regarded as a fixed value. It means

$$U_{0,s,t} = U^{REF}, s \in \mathcal{S}, t \in \mathcal{T} \quad (19)$$

where $U^{REF} = 1 p.u.$ is the voltage reference.

The voltages of other buses, except bus 0, should be maintained in a certain range, which is

$$\underline{U} \leq U_{i,s,t} \leq \bar{U}, i = 1, 2, \dots, N, s \in \mathcal{S}, t \in \mathcal{T} \quad (20)$$

where \underline{U} and \bar{U} are the minimal and maximal bus voltages.

The distribution system purchases electricity from the transmission system through bus 0. The electricity purchasing cost is formulated as

$$C_s^{EP} = \pi^{EP} \sum_{t \in \mathcal{T}} \sum_{(0,j) \in \mathcal{E}} P_{0j,s,t} \quad (21)$$

where $\pi^{EP} > 0$ is the unit electricity purchasing price. If the electricity purchasing cost is negative, it means that the distribution system sells surplus electricity to the transmission system.

2.4. Overall

Given the probability distribution of a typical scenario p_s , the total annual operational cost of the distribution system is

$$C^{OPER} = 365 \sum_{s \in \mathcal{S}} p_s \left(C_s^{EP} - R_s^{HT} + \sum_{i \in \mathcal{G}} C_{i,s}^G + \sum_{i \in \mathcal{V}} C_{i,s}^{PV} \right) \quad (22)$$

where p_s is the probability distribution of scenario s .

Then, the two-stage stochastic HPM planning problem is formulated as

$$\begin{aligned} \min & C^{INV} + C^{OPER} \\ \text{s.t.} & (1), (2), (6)–(9), (11), (12), (14), (17)–(20) \end{aligned} \quad (23)$$

When the number of typical scenarios increases, the above problem can be computationally expensive. In the following section, the benders' decomposition is utilized to efficiently solve the problem.

3. Benders' Decomposition-Based Solution Algorithm

In this section, we will propose a benders' decomposition algorithm to deal with the two-stage stochastic HPM planning model (23). The proposed Benders' decomposition-based solution algorithm is an iterative method. The problem (23) is divided into two types of problems, which are called the master problem and the subproblems, for typical scenarios. The master problem makes the decision of the HPM's capacity and location, while the subproblems simulate the operation of a distribution system in typical scenarios. The proposed algorithm successively solves the master problem and subproblems. Optimal cuts are built by solving subproblems and then added to the constraint of the master problem.

In the original problem (23), the decision variables without the subscript s belong to stage 1, while those with the subscript s belong to stage 2. Specifically, define the stage-1 decision vector as $x := \{ \bar{P}^{HPM}, u_i \}$ and the stage-2 decision vector in scenario s as $y_s := \{ P_{s,t}^{HPM}, P_{i,s,t}^{HPM}, n_{s,t}, P_{i,s,t}^G, P_{i,s,t}^{PV}, P_{ij,s,t}, Q_{ij,s,t}, U_{i,s,t}, P_{i,s,t} \}$.

Then, we have the compact form of the problem (23) as

$$\min_{x, \{y_s\}} \mathbf{b}^T \mathbf{x} + \sum_{s \in \mathcal{S}} \mathbf{c}_s^T \mathbf{y}_s \quad (24a)$$

$$\text{s.t. } \mathbf{x} \in \mathcal{X} \quad (24b)$$

$$A_s \mathbf{x} + B_s \mathbf{y}_s \leq \mathbf{d}_s, \forall s \in \mathcal{S} \quad (24c)$$

where \mathcal{X} represents the feasible region of stage-1 decision vector \mathbf{x} , A_s and B_s are constant matrices, and \mathbf{b} , \mathbf{c}_s , and \mathbf{d}_s are constant vectors.

Then, we formulate the subproblem and master problem during each iteration k of the benders' decomposition algorithm, respectively.

3.1. Formulation of Subproblem

Suppose that the capacity and location decision vector \mathbf{x}_k^* in stage 1 in iteration k is given by solving the master problem. The subproblem in scenario s for the stage-2 operation is formulated as

$$\min_{y_s} \mathbf{c}_s^T \mathbf{y}_s \quad (25a)$$

$$\text{s.t. } A_s \mathbf{x}_k^* + B_s \mathbf{y}_s \leq \mathbf{d}_s : \lambda_s \quad (25b)$$

where $\lambda_s \geq 0$ is the Lagrangian multiplier corresponding to the constraint (25b).

Instead of directly solving the primal problem (25), we focus on its dual problem

$$\max_{\lambda_s} (A_s \mathbf{x}_k^* - \mathbf{d}_s)^T \lambda_s \quad (26a)$$

$$\text{s.t. } \lambda_s \geq 0 \quad (26b)$$

$$B_s^T \lambda_s + \mathbf{c}_s = 0 \quad (26c)$$

After the subproblems in all scenarios are solved, we can formulate an upper bound (UB) for the optimal value of the original problem (24) as

$$\mathbf{b}^T \mathbf{x}_k^* + \sum_{s \in \mathcal{S}} (A_s \mathbf{x}_k^* - \mathbf{d}_s)^T \lambda_{s,k}^* \quad (27)$$

By solving the dual problem (26), we obtain the optimal solution denoted by $\lambda_{s,k}^*$. Using the optimal Lagrangian multiplier $\lambda_{s,k}^*$, we can formulate an optimal cut for the master problem as

$$(A_s \mathbf{x} - \mathbf{d}_s)^T \lambda_{s,k}^* \leq \theta_s \quad (28)$$

where θ_s is an auxiliary variable.

3.2. Formulation of Master Problem

Suppose that the optimal cuts in all typical scenarios until iteration k are given by solving the subproblems. The master problem for stage-1 planning is formulated as

$$\min_{x, \{\theta_s\}} \mathbf{b}^T \mathbf{x} + \sum_{s \in \mathcal{S}} \theta_s \quad (29a)$$

$$\text{s.t. } \mathbf{x} \in \mathcal{X} \quad (29b)$$

$$(A_s \mathbf{x} - \mathbf{d}_s)^T \lambda_{s,\kappa}^* \leq \theta_s, \forall s \in \mathcal{S}, \kappa = 1, 2, \dots, k \quad (29c)$$

By solving the master problem (29), we can obtain a new planning strategy \mathbf{x}_{k+1} . Note that the optimal value of problem (29) gives a lower bound (LB) for the optimal value of the original problem (24).

Compared to the original problem (24), the master problem only considers several optimal cuts instead of complicated constraints (24c). Thus, the computational complexity is significantly reduced.

3.3. Overall Algorithm

Based on the above formulations, we obtain the algorithm based on Benders' decomposition, called Algorithm 1, to solve the two-stage stochastic HPM planning problem.

Algorithm 1 Benders' decomposition for HPM planning

Input: Iterative index $k = 1$, error tolerance $\varepsilon > 0$, upper bound $UB = -\infty$, and lower bound $LB = +\infty$.

Output: Optimal HPM planning strategy \mathbf{x}^* .

S1 (Master problem): Solve the master problem (29). Denote by \mathbf{x}_k^* and F_k^* the optimal solution and optimal value of the master problem. Then update the HPM planning strategy as \mathbf{x}_k^* and the lower bound as $LB \leftarrow \max\{LB, F_k^*\}$.

S2 (Subproblem): For each scenario $s \in \mathcal{S}$, solve its subproblem (26). Denote by $\lambda_{s,k}^*$ the optimal Lagrangian multiplier of the subproblem for scenario s . Formulate an optimal cut

$$(A_s \mathbf{x} - \mathbf{d}_s)^T \lambda_{s,k}^* \leq \theta_s$$

and add it to the constraints of the master problem. After the subproblems of all scenarios are solved, update the upper bound as

$$UB \leftarrow \min \left\{ UB, \mathbf{b}^T \mathbf{x}_k^* + \sum_{s \in \mathcal{S}} (A_s \mathbf{x}_k^* - \mathbf{d}_s)^T \lambda_{s,k}^* \right\}.$$

S3 (Judgment): If $(UB - LB)/|UB| \leq \varepsilon$, terminate the iteration. The latest HPM planning strategy is output as the optimal one, i.e., $\mathbf{x}^* \leftarrow \mathbf{x}_k^*$. Otherwise, set $k \leftarrow k + 1$ and go to **S1**.

The convergence of the benders' decomposition algorithm has been proved in [42]. The master problem belongs to mixed-integer linear programming (MILP), while the subproblems are linear programming (LP) problems. Both can be solved by commercial solvers.

4. Data-Driven Scenario Reduction

In the two-stage stochastic HPM planning model (23), the typical scenarios and their probability distributions have been not determined. In this section, we propose a data-driven scenario reduction method to generate S typical scenarios from massive historical data. It is based on the K-means clustering method, a classic machine-learning approach.

In the proposed stochastic model (23), scenarios differ from the maximal power output profile of PV panel $\bar{P}_{i,s,t}^{PV}$ and the load profile $P_{i,s,t}^D, Q_{i,s,t}^D$. Note that the dimension of the aggregate vector is too large. We first reduce its dimension.

Assume that given scenario s , all loads have the same shape of the profile, i.e., there exist $\tilde{P}_{s,t}^D, \forall t \in \mathcal{T}$ and $\hat{P}_i^D, \hat{Q}_i^D, \forall i \in \mathcal{N}$ such that

$$P_{i,s,t}^D = \hat{P}_i^D \tilde{P}_{s,t}^D, \forall i \in \mathcal{N}, s \in \mathcal{S}, t \in \mathcal{T} \tag{30a}$$

$$Q_{i,s,t}^D = \hat{Q}_i^D \tilde{P}_{s,t}^D, \forall i \in \mathcal{N}, s \in \mathcal{S}, t \in \mathcal{T} \tag{30b}$$

and

$$0 \leq \tilde{P}_{s,t}^D \leq 1, \forall s \in \mathcal{S}, t \in \mathcal{T} \tag{31a}$$

$$\max_{s \in \mathcal{S}} \max_{t \in \mathcal{T}} \tilde{P}_{s,t}^D = 1 \tag{31b}$$

The sequence $\tilde{P}_{s,t}^D, t \in \mathcal{T}$ is called the normalized load profile in scenario s . In the same way, we can define the normalized maximal power output profile of PV panel $\tilde{P}_{s,t}^{PV}, t \in \mathcal{T}$ in scenario s . Let $w_s = \{\tilde{P}_{s,t}^D, \tilde{P}_{s,t}^{PV}, t \in \mathcal{T}\}$ denote the data vector in scenario s .

In practice, there are a large number of historical data denoted by $v_c, c = 1, 2, \dots, C$. The number of historical data C is much larger than that of the typical scenario S , i.e., $C \gg S$. We need to generate w_s from v_c . The main point of the K-means clustering method is to partition historical data into S clusters denoted by $C_s, s = 1, 2, \dots, S$. The centroid of each cluster is recognized as a typical scenario, i.e.,

$$w_s = \frac{1}{C_s} \sum_{c \in C_s} v_c \quad (32)$$

where C_s is the cardinality of set C_s .

Based on the K-means clustering method, we obtain the algorithm of partitioning historical data and generating typical scenarios named Algorithm 2. Ref. [47] proves the convergence of the K-means clustering method.

Algorithm 2 K-means clustering for scenario reduction

Input: Massive historical data $v_c, c = 1, 2, \dots, C$, randomized initial typical scenarios $w_s, s = 1, 2, \dots, S$, and empty clusters $C_s = \emptyset, s = 1, 2, \dots, S$.

Output: Typical scenarios w_s and their probability distributions p_s for $s = 1, 2, \dots, S$.

S1 (Partition): Clear the clusters $C_s, \forall s \in \mathcal{S}$ and then assign every historical data $v_c, c = 1, 2, \dots, C$ to the cluster with the nearest typical scenario, i.e.,

$$s_c^* = \arg \min_{s \in \mathcal{S}} \|v_c - w_s\|^2$$

$$C_{s_c^*} \leftarrow C_{s_c^*} \cup \{c\}$$

S2 (Update): Recalculate the typical scenarios by

$$w_s = \frac{1}{C_s} \sum_{c \in C_s} v_c, \forall s \in \mathcal{S}$$

and their probability distributions

$$p_s = \frac{C_s}{C}, \forall s \in \mathcal{S}.$$

S3 (Judgment): If the partitions no longer change, terminate the iteration and output the latest typical scenarios and their probability distributions. Otherwise, go to **S1**.

5. Case Study

5.1. Setup

The numerical experiments were carried out in a modified IEEE 33-bus distribution system integrated with five fuel generators and three PV panels [48]. The topology of the distribution system is shown in Figure 1. Given the whole year's historical data, applying Algorithm 2 can generate eight typical scenarios of the maximal power output profiles of the PV panel and the load profiles, which can be seen in Figures 2 and 3. The utilized K-means algorithm 2 is widely used for scenario reduction in the existing literature, e.g., Refs. [49–51]. For each day in the whole year's historical data, there is a maximum power output profile of the PV panel, where “maximum” means the PV output is not curtailed. The eight scenarios are selected by the K-means method because they are typical rather than maximal. In other words, the 365-day data are classified into eight types and each type can generate a typical scenario. In the K-means algorithm, the initial typical scenarios are randomly selected from the historical data. In the Benders' decomposition algorithm,

the error tolerance is set to $\epsilon = 10^{-6}$. The discount rate η^{DR} is 4.9%. The expected life span of HPM Y^{EP} is 10 years. The unit investment price of the HPM π^{HPM} is 350 USD/kW.

The hydrogen trading price π^{HTP} is 6 USD/kg. The hydrogen production rate η^{HPR} is 0.02 kg/kW.

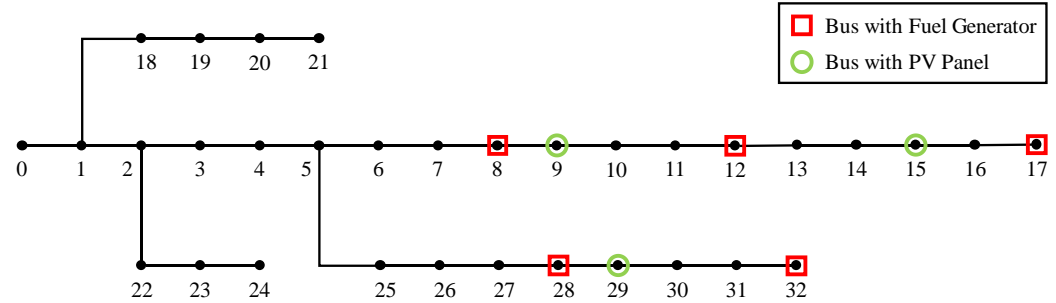


Figure 1. The topology of the IEEE 33-bus distribution system.

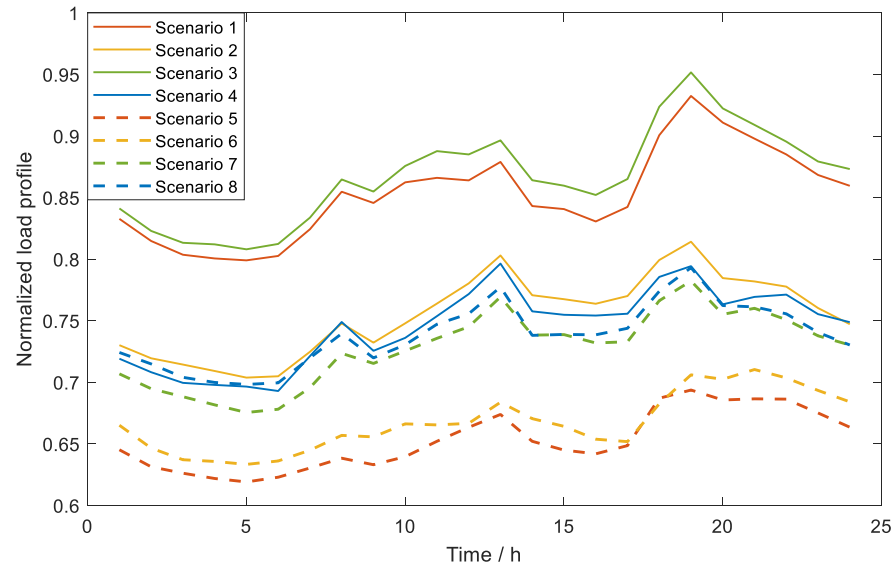


Figure 2. The normalized load profiles in typical scenarios.

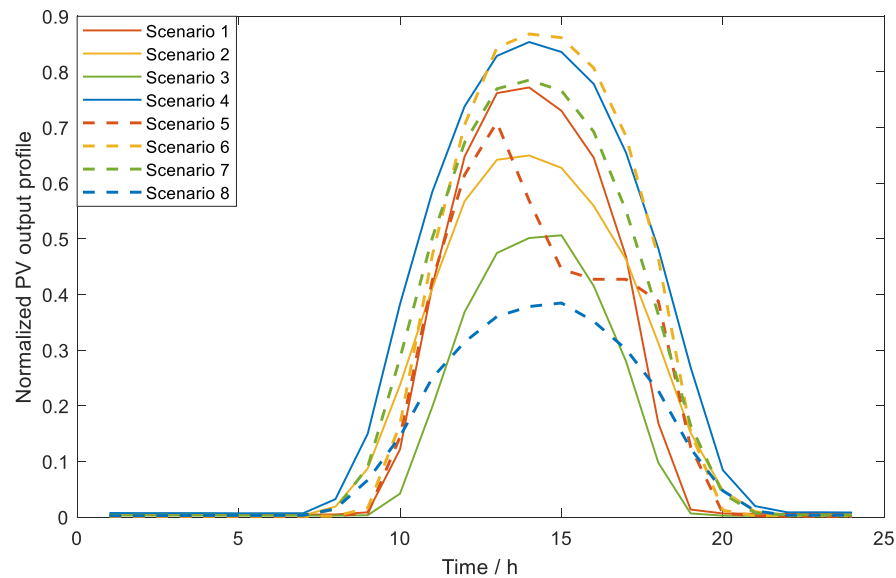


Figure 3. The normalized photovoltaic panel output profiles in typical scenarios.

5.2. Main Results

By applying the Benders' decomposition algorithm, we obtain an optimal HPM plan with a capacity of 545.53 kW and the location at bus 17. The detailed annual cost of the distribution system is shown in Table 1. Despite the annual investment cost of HPM, 0.25×10^5 \$, the distribution system can benefit from selling Hydrogen to factories, USD 2.68×10^5 . Table 1 also displays the detailed annual cost sheet of the distribution system if no HPM is installed. The relative reduction of the overall cost is 3.60%, which is a remarkably high improvement. The main difference between the costs with an HPM or not is that the redundant PV power is used to produce hydrogen instead of selling it to the transmission system. The burden of the power grid is significantly released.

Table 1. The annual balance sheet with/without Hydrogen production modules.

Condition	C^{EP} †	C^G †	C^{PV} †	C^{INV} †	R^{HT} †	Overall Cost †	Reduction
w/ HPM	−0.23	9.74	0.18	0.25	2.68	7.25	
w/o HPM	−2.39	9.60	0.31	0	0	7.52	3.60%

† The unit of cost/revenue is USD 10^5 . C^{EP} : electricity purchasing cost, where a negative value means selling electricity to the transmission system; C^G : operational cost of fuel generators; C^{PV} : penalty cost of PV curtailment; C^{INV} : investment cost of HPM; R^{HT} : revenue of Hydrogen trading.

Bus voltage is significantly concerned with the distribution system operator due to the high proportion of renewable energy. When PV outputs are sufficiently large, the bus voltage will reach the upper bound. The PV outputs have to be curtailed, which causes severe waste. In Figure 4, the red curve shows the voltage at bus 17 in typical scenario 7. It shows that from 10:00 to 18:00, the bus voltage reaches the upper bound, 1.05 p.u., which indicates the curtailment of PV output. After installing the HPM, as shown in the blue curve in Figure 4, the voltage congestion is greatly released. The surplus PV power is utilized to generate hydrogen, which effectively lightens the burden of distribution system operation and decreases the operational cost by selling hydrogen.

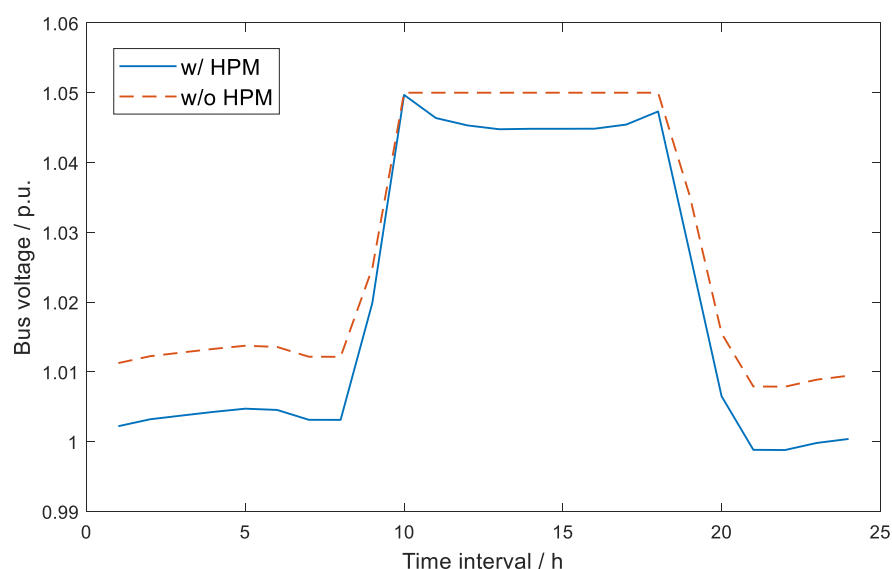


Figure 4. The voltage of bus 17 in scenario 7 with or without the Hydrogen production module.

The convergence of the Benders' decomposition algorithm is verified in Figure 5. As the number of optimal cuts grows, the restriction on the master problem becomes tighter. The lower bound obtained by the master problem increases, while the HPM investment plan becomes more and more rational. Meanwhile, the subproblems check the effect of the HPM investment plan and point out the direction of optimality by optimal cuts. When the

upper and lower bounds are equal, the latest HPM investment plan is recognized as the optimal one. Then, the Benders' decomposition algorithm terminates.

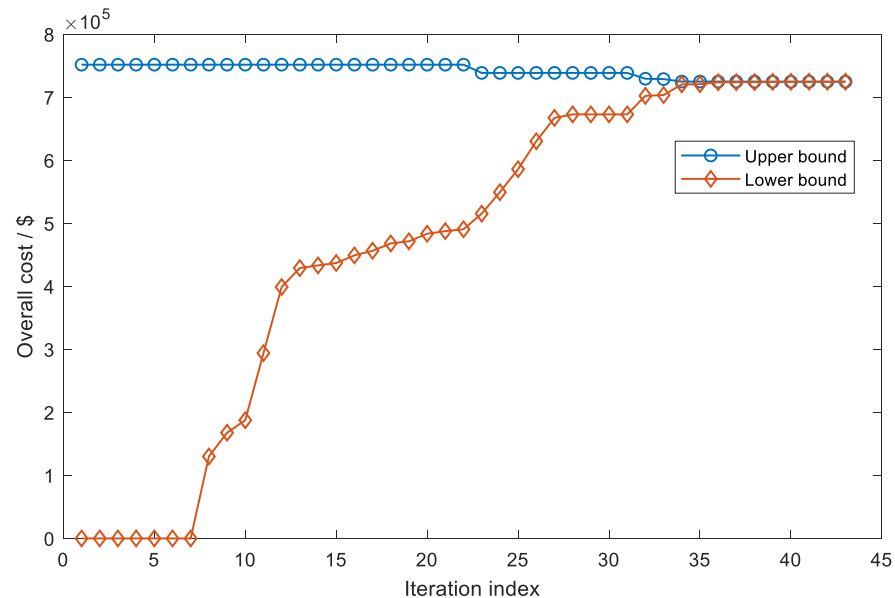


Figure 5. The lower and upper bounds of the overall cost during Benders' decomposition.

5.3. Sensitivity Analysis

Then, we verify the optimality of the HPM plan generated by the Benders' decomposition. Firstly, fix the HPM capacity of 545.53 kW and change the bus where it is connected. Figure 6 shows the curve of overall cost with different HPM locations. It is apparent that bus 17 has the minimal cost. Near-optimal locations are the buses near bus 17, which can be attributed to a relatively small electrical distance to PV panels. Then, the HPM can efficiently use abundant PV power.

Next, we will discuss the reason why the optimal location is bus 17. Figure 4 shows that the main challenge of the distribution system operation is the excessively high bus voltage due to the large-scale PVs. The HPM consumes surplus PV power to generate hydrogen and, meanwhile, restrains the rise of bus voltage. The location of the HPM will affect the distribution power flow and influence the bus voltage. From the topology of the IEEE 33-bus system in Figure 1, bus 17 is the farthest bus from bus 0. Ref. [52] shows that bus 17 has the largest mutual voltage-to-power injection sensitivity factor. Locating at bus 17 most effectively regulates the bus voltage.

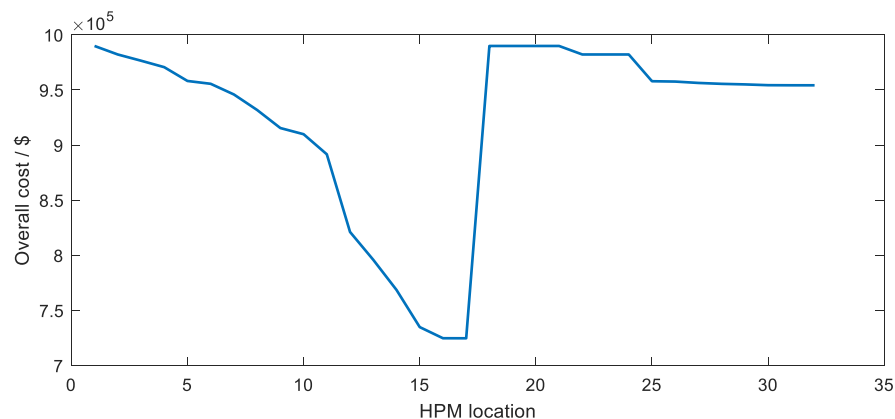


Figure 6. Curve of overall cost with different Hydrogen production module locations.

In addition, we fix the HPM location at bus 17 and change its capacity from 0 to 1000 kW. Figure 7 shows the curve of overall cost with different HPM capacities. It verifies

that the optimal HPM capacity is 545.53 kW. If the HPM capacity is too small, it is unable to consume sufficiently abundant PV power. When the HPM capacity is too large, there is no abundant PV power to consume, while the investment cost of HPM is kind of wasted. Moreover, a comparison between Figures 6 and 7 shows that the effect of location on the distribution system's overall cost is much larger than that of capacity. It is inspired to carefully select the location of HPM.

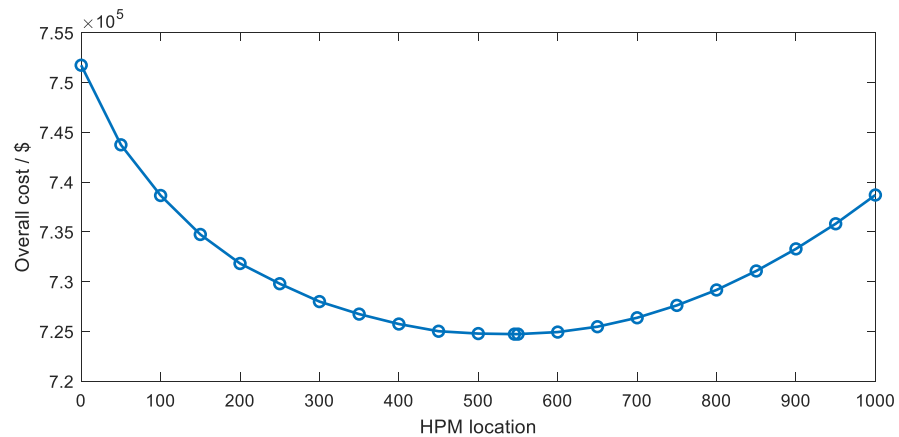


Figure 7. Curve of overall cost with different Hydrogen production module capacities.

6. Conclusions

In this paper, we propose a two-stage stochastic planning model for a hydrogen production module in distribution systems. Both the capacity and the location of the hydrogen production module are considered in the proposed model. The hydrogen production module can produce hydrogen and sell it to factories using abundant photovoltaic power. By investing in the hydrogen production module, the overall operational cost of the distribution system is significantly reduced and the power output of photovoltaic panels is efficiently utilized. Since the photovoltaic power is stochastic, we propose a data-driven algorithm to cluster massive historical data into several typical scenarios. It can remarkably reduce the scale of the proposed two-stage stochastic planning model. Additionally, a Benders' decomposition-based algorithm is proposed to efficiently solve the two-stage stochastic planning model, which is an iterative method with fast convergence speed. Numerical experiments verify the optimality of the hydrogen production module plan generated by the Benders' decomposition algorithm. After installing the HPM, the overall cost of the distribution system is reduced by 3.60%, which also reveals immense economic and environmental benefits. This work may inspire more studies on power system planning problems considering both the capacity and location of power equipment. At present, the proposed algorithm can only deal with linear problems. A significant improvement on the algorithm may enhance the behavior of the algorithm on non-linear problems for future research.

Author Contributions: Conceptualization, Z.L. and Y.S.; Methodology, Z.L., W.W. and Y.S.; Validation, X.C.; Investigation, Z.L. and Y.S.; Resources, W.W.; Writing—original draft, Z.L.; Writing—review & editing, W.W. and X.C.; Project administration, W.W.; Funding acquisition, Y.S. All authors have read and agreed to the published version of the manuscript.

Funding: This research was funded by Key R & D and Transformation Plan of Qinghai Province (2021-GX-109).

Data Availability Statement: Data are contained within the article.

Conflicts of Interest: The authors declare no conflict of interest.

References

1. Kovač, A.; Paranos, M.; Marciuš, D. Hydrogen in energy transition: A review. *Int. J. Hydrogen Energy* **2021**, *46*, 10016–10035. [[CrossRef](#)]
2. Chehade, Z.; Mansilla, C.; Lucchese, P.; Hilliard, S.; Proost, J. Review and analysis of demonstration projects on power-to-X pathways in the world. *Int. J. Hydrogen Energy* **2019**, *44*, 27637–27655. [[CrossRef](#)]
3. Sharma, S.; Ghoshal, S.K. Hydrogen the future transportation fuel: From production to applications. *Renew. Sustain. Energy Rev.* **2015**, *43*, 1151–1158. [[CrossRef](#)]
4. Kwak, J.; Lee, H.; Park, S.; Park, J.; Jung, S. Risk Assessment of a Hydrogen Refueling Station in an Urban Area. *Energies* **2023**, *16*, 3963. [[CrossRef](#)]
5. Mouli-Castillo, J.; Heinemann, N.; Edlmann, K. Mapping geological hydrogen storage capacity and regional heating demands: An applied UK case study. *Appl. Energy* **2021**, *283*, 116348. [[CrossRef](#)]
6. Cao, Q.; Li, B.; Jia, M.; Shen, C. The Design of By-product Hydrogen Supply Chain Considering Large-scale Storage and Chemical Plants: A Game Theory Perspective. *arXiv* **2022**, arXiv:2211.03118.
7. Qadrdan, M.; Abeysekera, M.; Chaudry, M.; Wu, J.; Jenkins, N. Role of power-to-gas in an integrated gas and electricity system in Great Britain. *Int. J. Hydrogen Energy* **2015**, *40*, 5763–5775. [[CrossRef](#)]
8. Schmidt, O.; Gambhir, A.; Staffell, I.; Hawkes, A.; Nelson, J.; Few, S. Future cost and performance of water electrolysis: An expert elicitation study. *Int. J. Hydrogen Energy* **2017**, *42*, 30470–30492. [[CrossRef](#)]
9. Brauns, J.; Turek, T. Alkaline water electrolysis powered by renewable energy: A review. *Processes* **2020**, *8*, 248. [[CrossRef](#)]
10. Rambhujun, N.; Salman, M.S.; Wang, T.; Prathana, C.; Sapkota, P.; Costalin, M.; Lai, Q.; Aguey-Zinsou, K.F. Renewable hydrogen for the chemical industry. *MRS Energy Sustain.* **2020**, *7*, E33. [[CrossRef](#)]
11. Little, M.; Thomson, M.; Infield, D. Electrical integration of renewable energy into stand-alone power supplies incorporating hydrogen storage. *Int. J. Hydrogen Energy* **2007**, *32*, 1582–1588. [[CrossRef](#)]
12. Nasri, S.; Sami, B.S.; Cherif, A. Power management strategy for hybrid autonomous power system using hydrogen storage. *Int. J. Hydrogen Energy* **2016**, *41*, 857–865. [[CrossRef](#)]
13. Wei, C.; Xia, Z.; Haihua, W.; Xuedong, H.; Le, P. Optimal Capacity Allocation of Hydrogen Production System Participating Peak Regulation for Auxiliary with Thermal Power Plant. *Distrib. Energy Resour.* **2020**, *5*, 15–20.
14. Morel, J.; Obara, S.; Sato, K.; Mikawa, D.; Watanabe, H.; Tanaka, T. Contribution of a hydrogen storage-transportation system to the frequency regulation of a microgrid. In Proceedings of the 2015 IEEE International Conference on Renewable Energy Research and Applications (ICRERA), Palermo, Italy, 22–25 November 2015; pp. 510–514.
15. Sun, D.; Zheng, W.; Yu, J.; Li, J. Research on the Primary Frequency Regulation Control Strategy of a Wind Storage Hydrogen-Generating Power Station. *Electronics* **2022**, *11*, 3669. [[CrossRef](#)]
16. Dehghanian, P.; Hosseini, S.H.; Moeini-Aghaie, M.; Arabali, A. Optimal siting of DG units in power systems from a probabilistic multi-objective optimization perspective. *Int. J. Electr. Power Energy Syst.* **2013**, *51*, 14–26. [[CrossRef](#)]
17. Liu, S.; Messina, A.; Vittal, V. A normal form analysis approach to siting power system stabilizers (PSSs) and assessing power system nonlinear behavior. *IEEE Trans. Power Syst.* **2006**, *21*, 1755–1762. [[CrossRef](#)]
18. Gözel, T.; Hocaoglu, M.H. An analytical method for the sizing and siting of distributed generators in radial systems. *Electr. Power Syst. Res.* **2009**, *79*, 912–918. [[CrossRef](#)]
19. Arabali, A.; Ghofrani, M.; Etezadi-Amoli, M.; Fadali, M.S. Stochastic performance assessment and sizing for a hybrid power system of solar/wind/energy storage. *IEEE Trans. Sustain. Energy* **2013**, *5*, 363–371. [[CrossRef](#)]
20. Zeng, Q.; Fang, J.; Chen, Z.; Li, J.; Zhang, B. A multistage coordinative optimization for siting and sizing P2G plants in an integrated electricity and natural gas system. In Proceedings of the 2016 IEEE International Energy Conference (ENERGYCON), Leuven, Belgium, 4–8 April 2016; pp. 1–6.
21. Wang, S.; Yu, J. Optimal sizing of the CAES system in a power system with high wind power penetration. *Int. J. Electr. Power Energy Syst.* **2012**, *37*, 117–125. [[CrossRef](#)]
22. Carpinelli, G.; Celli, G.; Pilo, F.; Russo, A. Distributed generation siting and sizing under uncertainty. In Proceedings of the 2001 IEEE Porto Power Tech Proceedings (Cat. No. 01EX502), Porto, Portugal, 10–13 September 2001; Volume 4, p. 7.
23. Liu, Z.; Wen, F.; Ledwich, G. Optimal siting and sizing of distributed generators in distribution systems considering uncertainties. *IEEE Trans. Power Deliv.* **2011**, *26*, 2541–2551. [[CrossRef](#)]
24. Serrano-Arévalo, T.I.; Tovar-Facio, J.; Ponce-Ortega, J.M. Optimal Incorporation of Intermittent Renewable Energy Storage Units and Green Hydrogen Production in the Electrical Sector. *Energies* **2023**, *16*, 2609. [[CrossRef](#)]
25. Eladl, A.A.; El-Affifi, M.I.; Saeed, M.A.; El-Saadawi, M.M. Optimal operation of energy hubs integrated with renewable energy sources and storage devices considering CO₂ emissions. *Int. J. Electr. Power Energy Syst.* **2020**, *117*, 105719. [[CrossRef](#)]
26. Maleki, A.; Rosen, M.A.; Pourfayaz, F. Optimal operation of a grid-connected hybrid renewable energy system for residential applications. *Sustainability* **2017**, *9*, 1314. [[CrossRef](#)]
27. Vivas, F.; De las Heras, A.; Segura, F.; Andújar, J. A review of energy management strategies for renewable hybrid energy systems with hydrogen backup. *Renew. Sustain. Energy Rev.* **2018**, *82*, 126–155. [[CrossRef](#)]
28. García, P.; García, C.A.; Fernández, L.M.; Llorens, F.; Jurado, F. ANFIS-based control of a grid-connected hybrid system integrating renewable energies, hydrogen and batteries. *IEEE Trans. Ind. Inform.* **2013**, *10*, 1107–1117. [[CrossRef](#)]

29. Rouholamini, M.; Mohammadian, M. Energy management of a grid-tied residential-scale hybrid renewable generation system incorporating fuel cell and electrolyzer. *Energy Build.* **2015**, *102*, 406–416. [[CrossRef](#)]
30. Eriksson, E.; Gray, E.M. Optimization and integration of hybrid renewable energy hydrogen fuel cell energy systems—A critical review. *Appl. Energy* **2017**, *202*, 348–364. [[CrossRef](#)]
31. Hotza, D.; Da Costa, J.D. Fuel cells development and hydrogen production from renewable resources in Brazil. *Int. J. Hydrogen Energy* **2008**, *33*, 4915–4935. [[CrossRef](#)]
32. Esposito, D.V. Membraneless electrolyzers for low-cost hydrogen production in a renewable energy future. *Joule* **2017**, *1*, 651–658. [[CrossRef](#)]
33. Ciupageanu, D.A.; Barelli, L.; Lazaroiu, G. Real-time stochastic power management strategies in hybrid renewable energy systems: A review of key applications and perspectives. *Electr. Power Syst. Res.* **2020**, *187*, 106497. [[CrossRef](#)]
34. Bu, S.; Yu, F.R.; Liu, P.X. Stochastic unit commitment in smart grid communications. In Proceedings of the 2011 IEEE Conference on Computer Communications Workshops (INFOCOM WKSHPs), Shanghai, China, 10–15 April 2011; pp. 307–312.
35. Bassamzadeh, N.; Ghanem, R. Multiscale stochastic prediction of electricity demand in smart grids using Bayesian networks. *Appl. Energy* **2017**, *193*, 369–380. [[CrossRef](#)]
36. Bertsimas, D.; Litvinov, E.; Sun, X.A.; Zhao, J.; Zheng, T. Adaptive robust optimization for the security constrained unit commitment problem. *IEEE Trans. Power Syst.* **2012**, *28*, 52–63. [[CrossRef](#)]
37. Su, Y.; Liu, F.; Wang, Z.; Zhang, Y.; Li, B.; Chen, Y. Multi-Stage Robust Dispatch Considering Demand Response Under Decision-Dependent Uncertainty. *IEEE Trans. Smart Grid* **2022**, *14*, 2786–2797. [[CrossRef](#)]
38. Verastegui, F.; Lorca, A.; Olivares, D.E.; Negrete-Pincetic, M.; Gazmuri, P. An adaptive robust optimization model for power systems planning with operational uncertainty. *IEEE Trans. Power Syst.* **2019**, *34*, 4606–4616. [[CrossRef](#)]
39. Xiong, P.; Jirutitijaroen, P.; Singh, C. A distributionally robust optimization model for unit commitment considering uncertain wind power generation. *IEEE Trans. Power Syst.* **2016**, *32*, 39–49. [[CrossRef](#)]
40. Guo, Y.; Baker, K.; Dall’Anese, E.; Hu, Z.; Summers, T. Stochastic optimal power flow based on data-driven distributionally robust optimization. In Proceedings of the 2018 IEEE Annual American Control Conference (ACC), Milwaukee, WI, USA, 27–29 June 2018; pp. 3840–3846.
41. Ma, H.; Jiang, R.; Yan, Z. Distributionally robust co-optimization of power dispatch and do-not-exceed limits. *IEEE Trans. Power Syst.* **2019**, *35*, 887–897. [[CrossRef](#)]
42. Sahinidis, N.; Grossmann, I.E. Convergence properties of generalized Benders decomposition. *Comput. Chem. Eng.* **1991**, *15*, 481–491. [[CrossRef](#)]
43. Soares, J.; Canizes, B.; Ghazvini, M.A.F.; Vale, Z.; Venayagamoorthy, G.K. Two-stage stochastic model using benders’ decomposition for large-scale energy resource management in smart grids. *IEEE Trans. Ind. Appl.* **2017**, *53*, 5905–5914. [[CrossRef](#)]
44. Zhang, Y.; Wang, J.; Zeng, B.; Hu, Z. Chance-constrained two-stage unit commitment under uncertain load and wind power output using bilinear benders decomposition. *IEEE Trans. Power Syst.* **2017**, *32*, 3637–3647. [[CrossRef](#)]
45. Baran, M.E.; Wu, F.F. Optimal capacitor placement on radial distribution systems. *IEEE Trans. Power Deliv.* **1989**, *4*, 725–734. [[CrossRef](#)]
46. Zhu, H.; Liu, H.J. Fast local voltage control under limited reactive power: Optimality and stability analysis. *IEEE Trans. Power Syst.* **2015**, *31*, 3794–3803. [[CrossRef](#)]
47. Krishna, K.; Murty, M.N. Genetic K-means algorithm. *IEEE Trans. Syst. Man Cybern. Part B* **1999**, *29*, 433–439. [[CrossRef](#)] [[PubMed](#)]
48. Li, B.; Chen, Y.; Wei, W.; Wang, Z.; Mei, S. Online coordination of LNG tube trailer dispatch and resilience restoration of integrated power-gas distribution systems. *IEEE Trans. Smart Grid* **2022**, *13*, 1938–1951. [[CrossRef](#)]
49. Lee, D.; Baek, S.; Sung, K. Modified k-means algorithm for vector quantizer design. *IEEE Signal Process. Lett.* **1997**, *4*, 2–4.
50. Charalampidis, D. A modified k-means algorithm for circular invariant clustering. *IEEE Trans. Pattern Anal. Mach. Intell.* **2005**, *27*, 1856–1865. [[CrossRef](#)]
51. Singh, R.V.; Bhatia, M.S. Data clustering with modified K-means algorithm. In Proceedings of the 2011 IEEE International Conference on Recent Trends in Information Technology (ICRTIT), Chennai, India, 3–5 June 2011; pp. 717–721.
52. Zhou, X.; Farivar, M.; Liu, Z.; Chen, L.; Low, S.H. Reverse and forward engineering of local voltage control in distribution networks. *IEEE Trans. Autom. Control.* **2020**, *66*, 1116–1128. [[CrossRef](#)]

Disclaimer/Publisher’s Note: The statements, opinions and data contained in all publications are solely those of the individual author(s) and contributor(s) and not of MDPI and/or the editor(s). MDPI and/or the editor(s) disclaim responsibility for any injury to people or property resulting from any ideas, methods, instructions or products referred to in the content.